

ISOTROPIC LUMINOSITY INDICATORS IN A COMPLETE AGN SAMPLE

ALEKSANDAR M. DIAMOND-STANIC¹, GEORGE H. RIEKE¹, JANE R. RIGBY²

Published in The Astrophysical Journal

ABSTRACT

The [O IV] $\lambda 25.89 \mu\text{m}$ line has been shown to be an accurate indicator of active galactic nucleus (AGN) intrinsic luminosity in that it correlates well with hard (10–200 keV) X-ray emission. We present measurements of [O IV] for 89 Seyfert galaxies from the unbiased revised Shapley–Ames (RSA) sample. The [O IV] luminosity distributions of obscured and unobscured Seyferts are indistinguishable, indicating that their intrinsic AGN luminosities are quite similar and that the RSA sample is well suited for tests of the unified model. In addition, we analyze several commonly used proxies for AGN luminosity, including [O III] $\lambda 5007 \text{\AA}$, 6 cm radio, and 2–10 keV X-ray emission. We find that the radio luminosity distributions of obscured and unobscured AGNs show no significant difference, indicating that radio luminosity is a useful isotropic luminosity indicator. However, the observed [O III] and 2–10 keV luminosities are systematically smaller for obscured Seyferts, indicating that they are not emitted isotropically.

Subject headings: galaxies: active, galaxies: nuclei, galaxies: Seyfert

1. INTRODUCTION

Many differences among active galactic nuclei (AGNs) are explained in terms of the line of sight to the supermassive black hole, such that an object will be classified as unobscured (type 1) if the central continuum source and broad-line region are directly visible, or as obscured (type 2) if large amounts of gas and dust block the central region. Unification schemes (e.g., Antonucci 1993) often invoke obscuring material in a torus geometry, such that the observed spectral energy distribution depends solely on viewing angle and the covering fraction of the torus sets the ratio of obscured to unobscured objects. This paradigm has been challenged by suggestions that the obscured-to-unobscured ratio varies as a function of luminosity (e.g., Ueda et al. 2003; Steffen et al. 2003; La Franca et al. 2005) and that some low-luminosity AGNs may not have broad-line regions at all (e.g., Tran 2003; Bianchi et al. 2008; Brightman & Nandra 2008).

To test models for the geometry of the obscuring material and the fundamental differences between type 1 and type 2 AGNs, one needs an unbiased, well-understood sample of objects that includes both low-luminosity and highly obscured sources. The spectroscopically selected, galaxy-magnitude-limited sample drawn from the revised Shapley–Ames catalog (RSA; Shapley & Ames 1932; Sandage & Tammann 1987) meets these criteria (Maiolino & Rieke 1995; Ho et al. 1997), and is well suited to probe basic predictions of AGN behavior. For example, if the sample is truly unbiased and the unified model is correct, the intrinsic AGN properties of the obscured and unobscured members should be the same.

In this paper, we consider 89 Seyferts from Maiolino & Rieke (1995) and Ho et al. (1997) drawn from the parent sample of galaxies with $B_T \leq 13$.³ This sample (see Table 1) includes 18 Seyfert 1s (type 1.0–1.5,

hereafter Sy1s) and 71 Seyfert 2s (type 1.8–2, hereafter Sy2s). We use it to probe whether there is a systematic luminosity difference between obscured and unobscured AGNs. Such a difference would be expected if AGN obscuration were luminosity dependent (e.g., Lawrence 1991) or if there existed a significant population of low-luminosity AGNs that lack a broad-line region (e.g., Laor 2003; Nicastro et al. 2003) in the sense that Sy2s would be disproportionately represented at faint luminosities. We determine the AGN luminosity through measurements of the [O IV] emission line at $25.89 \mu\text{m}$ (ionization potential 54.9 eV, critical density 10^4 cm^{-3}), which has been established as an accurate luminosity indicator by Meléndez et al. (2008a) and Rigby et al. (2009) by comparison to hard ($E > 10 \text{ keV}$) X-rays. We also compile measurements from the literature of quantities that are thought to be luminosity indicators, including [O III] $\lambda 5007 \text{\AA}$, 2–10 keV X-ray, and 6 cm radio emission, to determine which are in fact isotropically emitted.

2. DATA

We gather data from the *Spitzer Space Telescope* (Werner et al. 2004) archive taken with the Infrared Spectrograph (IRS; Houck et al. 2004) in the first order of the Long-Low module (LL1; $\lambda = 19.5\text{--}38.0 \mu\text{m}$). The slit size for this order is $10.7'' \times 168''$ and the resolution is $R = 64\text{--}128$. For data taken in staring mode, we begin our analysis on the post-basic calibrated data produced by the *Spitzer* Science Center pipeline and compute a weighted average of the one-dimensional spectra extracted at each of the nod positions. For data taken in mapping mode, we begin our analysis with the basic calibrated data and use the CUBISM software (Smith et al. 2007) to combine two-dimensional images and extract one-dimensional spectra. To obtain flux calibration appropriate for point sources, we disable the FLUXCON and SLCF options within CUBISM, and use $10.7 \times 35.2''$ apertures centered on the nucleus of the galaxy; this aperture corresponds to the LL1 slit size ($10.7''$) and the default point-source extraction aperture size at $26 \mu\text{m}$ ($35.2''$).

For each spectrum, we fit a power law to the continuum using the rest-frame wavelength regions $24.75\text{--}25.5 \mu\text{m}$ and $26.5\text{--}27 \mu\text{m}$. We then fit a Gaussian to the [O IV] line and

¹ Steward Observatory, University of Arizona, 933 North Cherry Avenue, Tucson, AZ, 85721, USA; adiamond@as.arizona.edu

² Observatories, Carnegie Institution of Washington, 813 Santa Barbara Street, Pasadena, CA 91101, USA

³ We do not include two galaxies classified as Seyferts by Ho et al. (1997), NGC185 and NGC676. The former is a dwarf spheroidal galaxy without a well-defined nucleus (Ho et al. 1995; Ho & Ulvestad 2001), and the latter is contaminated by a bright star $5''$ from its nucleus.

calculate the error on the flux measurement using the uncertainty in the five pixels closest to $\lambda_{\text{rest}} = 25.89 \mu\text{m}$ and the rms of the continuum fit in the wavelength regions mentioned above. For cases where this method yields a $< 5\sigma$ line detection, we inspect the spectrum visually to determine whether the line is confidently detected. If there is not a clear detection, we calculate a conservative upper limit by adding 3σ to the best-fit flux. The IRS LL1 data for NGC1068, CIRCINUS, and NGC4945 are saturated, so we take fluxes from ISO-SWS spectra published by Sturm et al. (2002) and Spoon et al. (2000).

A source of uncertainty for [O IV] fluxes measured from low-resolution IRS spectra is contamination by [Fe II] $\lambda 25.99 \mu\text{m}$ (ionization potential 7.9 eV) emission associated with star formation. Spectra from the IRS Long-High module (LH, $R \sim 600$) are available for 68/70 of the Seyferts with an LL1 line detection, so we are able to measure the amount of [Fe II] contamination. We analyze the post-basic calibrated data from LH order 15 ($\lambda = 25.0 - 27.4 \mu\text{m}$) and fit a Gaussian to each of the two lines. For sources with LL1 equivalent widths (EWs) greater than $0.10 \mu\text{m}$, the median value for the sample, we find that the [Fe II] contribution is small ($< 15\%$ in all cases). Among the sources with lower EWs, most still have $< 25\%$ [Fe II] contributions, but a few are actually dominated by [Fe II] (NGC3079, NGC4579, NGC4594, NGC5005). We apply a correction to the LL1 [O IV] measurements for all sources that have an LH [Fe II] detection. The [O IV] fluxes and uncertainties are listed in Table 1.

For the purpose of determining whether sources with large [Fe II] contributions can be identified without high-resolution data, we consider the [Ne II] $\lambda 12.81 \mu\text{m}$ (ionization potential 21.6 eV) emission, which is also associated with star formation. Inspection of IRS data from the first order of the Short-Low module ($\lambda = 7.4 - 14.5 \mu\text{m}$) indicates that sources with $> 15\%$ [Fe II] contributions also have strong [Ne II] lines; the ratio of [Ne II] to [O IV]+[Fe II] for these sources is always unity or greater. Indeed, all 19 sources with $> 15\%$ [Fe II] contributions can be identified as having both [O IV] $\text{EW} \leq 0.1 \mu\text{m}$ and $[\text{Ne II}]/[\text{O IV}] \geq 1$. There are, however, an additional eight sources that meet these criteria, but only have $\sim 10\%$ [Fe II] contributions.

Utilizing the NED⁴ and HEASARC⁵ databases, we searched the literature to gather [O III] $\lambda 5007 \text{\AA}$ emission-line fluxes, 2–10 keV X-ray fluxes, and 6 cm radio flux densities. These values and the corresponding references are included in Table 1. When multiple values were available, we gave preference to measurements with smaller beam sizes that isolate the nuclear emission from that of the host galaxy. All values are observed quantities that have not been corrected for extinction. For the galaxies with extinction-corrected [O III] fluxes published by Vaceli et al. (1997) and Winkler (1992), we calculated observed [O III] fluxes based on the assumed dust reddening. All sources have published 6 cm flux densities or upper limits, and all except NGC4945 have published [O III] fluxes. The X-ray coverage of the sample is less complete, but 72/89 galaxies have published 2–10 keV fluxes, and an additional nine sources have unpublished XMM-Newton archival data. For these nine sources, we use European Photon Imaging Camera count rates and flux measurements in the 2.0–4.5 keV and 4.5–12.0 keV bands from the XMM-Newton

⁴ <http://nedwww.ipac.caltech.edu/>.

⁵ <http://heasarc.gsfc.nasa.gov/>.

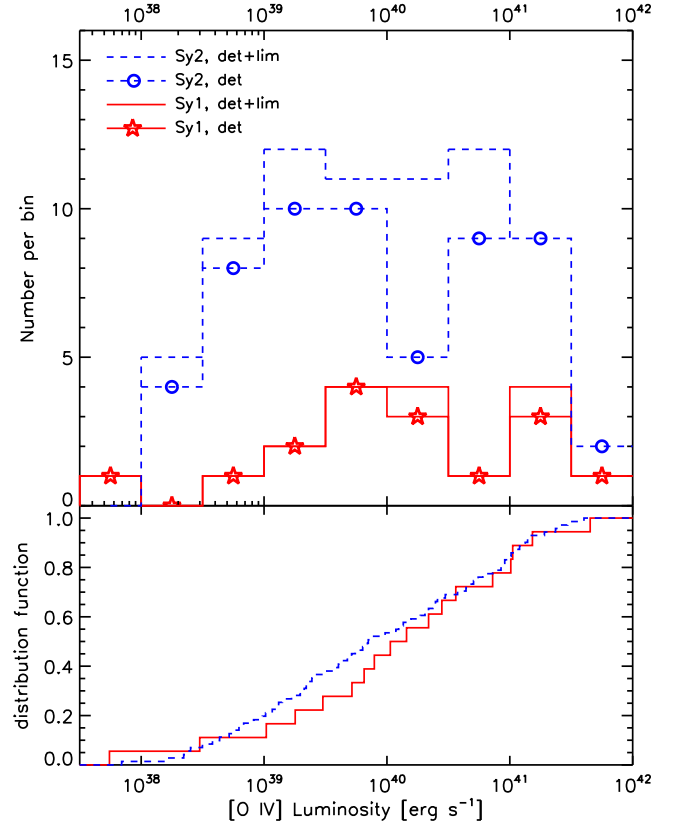


FIG. 1.— The distribution of [O IV] $\lambda 25.89 \mu\text{m}$ luminosities for Seyfert galaxies in the RSA sample. The top panel shows histograms for Sy2 detections and upper limits (dashed blue line), Sy2 detections (dashed blue line marked by blue circles), Sy1 detections and upper limits (solid red line), and Sy1 detections (solid red line marked by red stars). The bottom panel shows the empirical distribution functions for Sy2s and Sy1s. The distributions are not statistically distinguishable.

Serendipitous Source Catalogue (Watson et al. 2009) along with the power-law photon index Γ inferred using PIMMS v3.9i⁶ to estimate 2–10 keV fluxes. More complete X-ray spectral analysis for these sources is deferred to future work.⁷

For galaxies studied by Ho et al. (1997), we use distances from their Table 10 with exceptions for NGC1058, NGC3031, NGC4258, NGC4395, and NGC5194 (see Table 1). For the remaining galaxies we use distances from NED that are calculated assuming $H_0 = 73 \text{ km}^{-1} \text{ s}^{-1} \text{ Mpc}^{-1}$ and velocity-field corrected using the Mould et al. (2000) model, which includes the influence of the Virgo cluster, the Great Attractor, and the Shapley supercluster.

3. COMPARISON OF ISOTROPIC AGN INDICATORS

Commonly proposed isotropic indicators of AGN luminosity include [O III] $\lambda 5007 \text{\AA}$, radio, and hard X-ray emission. Our [O IV] $\lambda 25.89 \mu\text{m}$ measurements and the data we have gathered from the literature let us compare these indicators in obscured and unobscured members of the RSA Seyfert sam-

⁶ <http://heasarc.nasa.gov/Tools/w3pimms.html>.

⁷ However, inspection of pipeline products from XMM-Newton Science Archive Version 5.0 (<http://xmm.esac.esa.int/xsa/>) reveals a strong (EW $> 1 \text{ keV}$) Fe K α emission line in the spectrum of NGC7479, indicative of a Compton-thick source.

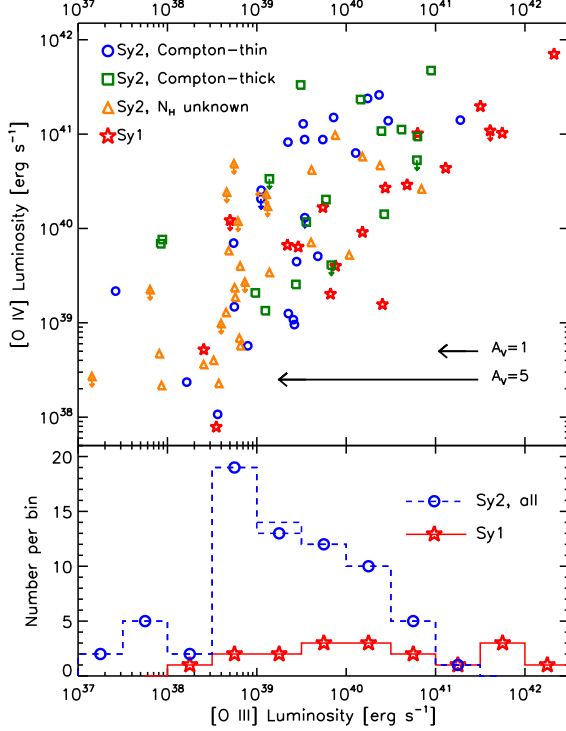


FIG. 2.— Top panel: The relationship between [O IV] $\lambda 25.89 \mu\text{m}$ and [O III] $\lambda 5007 \text{\AA}$ luminosities. No extinction corrections have been applied. Sy1s are indicated by red stars, Compton-thin ($N_H < 10^{24} \text{ cm}^{-2}$) Sy2s are indicated by blue circles, Compton-thick ($N_H > 10^{24} \text{ cm}^{-2}$) Sy2s are indicated by green squares, and Sy2s with unknown column densities are indicated by orange triangles. While most Sy1s have order unity [O IV]/[O III] luminosity ratios, a number of Sy2s are significantly brighter in [O IV] by up to a factor of ~ 100 . We interpret this as being due to large host galaxy obscuration in some Sy2s. The arrows indicate the effects of extinction on the observed [O III] luminosity for $A_V = 1$ and $A_V = 5$. Bottom panel: the distribution of [O III] luminosities, with histogram colors and symbols as in Figure 1. The distributions for Sy1s and Sy2s are statistically different with $p < 0.005$.

ple.

We present the distribution of [O IV] luminosities in Figure 1; the distributions for Sy2s and Sy1s are quite similar. We utilize two-sample statistical tests that take upper limits into account (Feigelson & Nelson 1985), and find that the two samples are consistent with being drawn from the same parent distribution (see Table 2). When the Sy2s are grouped by X-ray column density, we find that both Compton-thin ($N_H < 10^{24} \text{ cm}^{-2}$) and Compton-thick ($N_H > 10^{24} \text{ cm}^{-2}$) Sy2s are statistically indistinguishable from Sy1s. The only statistically significant difference is found when comparing the Sy1s to the Sy2s without published column densities. This latter group is biased towards X-ray-faint sources that do not have enough counts for a column density measurement and probably tend to have lower intrinsic luminosities. In Figure 1, the largest deviation between the Sy1 and Sy2 distributions occurs in the $L_{[\text{O IV}]} = 10^{38.5} - 10^{40} \text{ erg s}^{-1}$ range, where these “ N_H unknown” Sy2s are concentrated. We emphasize that this deviation does not produce a statistically significant effect in the overall Sy2 sample, and is less pronounced than the apparent excess of low-luminosity ($L_{[\text{O IV}]} < 10^{40.5} \text{ erg s}^{-1}$) Sy2s relative to Sy1s seen in a hybrid sample of local Seyfert galaxies by Meléndez et al. (2008).

The [O III] luminosities are presented in Figure 2 and the re-

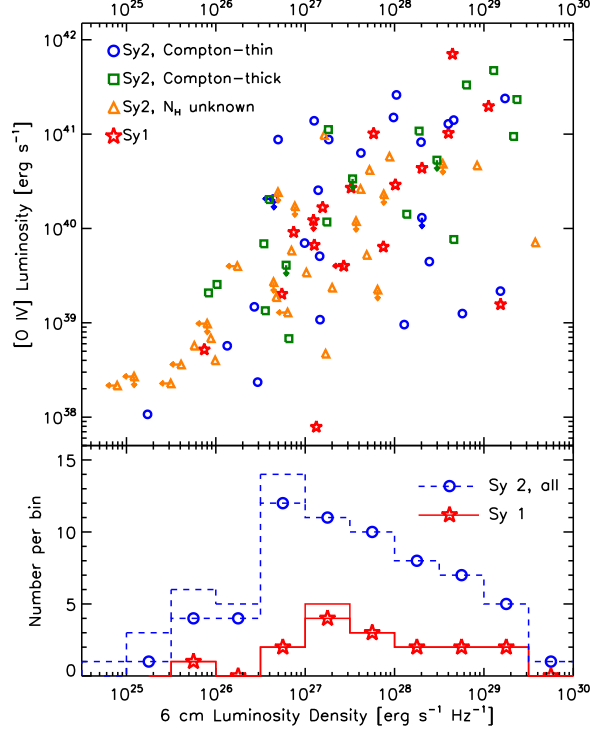


FIG. 3.— Top panel: The relationship between [O IV] $\lambda 25.89 \mu\text{m}$ and 6 cm radio luminosities. The symbols are as in Figure 2. There is large scatter in this relationship, but also significant overlap between the various Seyfert types. Bottom panel: The distribution of 6 cm luminosities, with histogram colors and symbols as in Figure 1. The distributions for Sy1s and Sy2s are not statistically distinguishable.

sults of statistical tests are presented in Table 3. We find a statistically significant difference between the [O III] luminosity distributions of Sy1s and Sy2s; the probability that the two samples are drawn from the same parent distribution is $p < 0.005$. While Sy1s tend to have observed [O IV]/[O III] ratios of order unity, a sizable fraction of the Sy2s have significantly larger ratios (e.g., all 21 objects with both lines detected and $[\text{O IV}]/[\text{O III}] > 5$ are Sy2s; see the upper-left side of Figure 2). We interpret this behavior as being due to larger host galaxy obscuration towards the narrow-line region in Sy2s. Similarly, Haas et al. (2005) invoke optical extinction to explain the higher [O IV]/[O III] ratios in FR2 radio galaxies relative to quasars. The fluxes in Table 1 are not corrected for extinction, and in some cases the [O III] extinction corrections implied by optical diagnostics such as the Balmer decrement are substantial (e.g., Bassani et al. 1999). However, applying such a correction does not always yield a satisfactory result — two of the galaxies with the largest [O IV]/[O III] ratios, NGC3281 and NGC5128, only exhibit moderate Balmer reddening $H\alpha/H\beta \simeq 6$. This corresponds to extinction by a factor of $\simeq 10$ at 5007 Å, not sufficient to explain the extreme values $[\text{O IV}]/[\text{O III}] \simeq 100$. This discrepancy can be explained if [O IV] is detected from heavily extinguished regions that are optically thick ($\tau >> 1$) at visible wavelengths, while the [O III], H α , and H β lines are detected exclusively from less-extinguished regions, resulting in a shallower observed Balmer decrement that underestimates the true extinction. Interestingly, there is no statistically significant difference between the [O III] distribution of Sy1s and Compton-thick Sy2s, but this is because

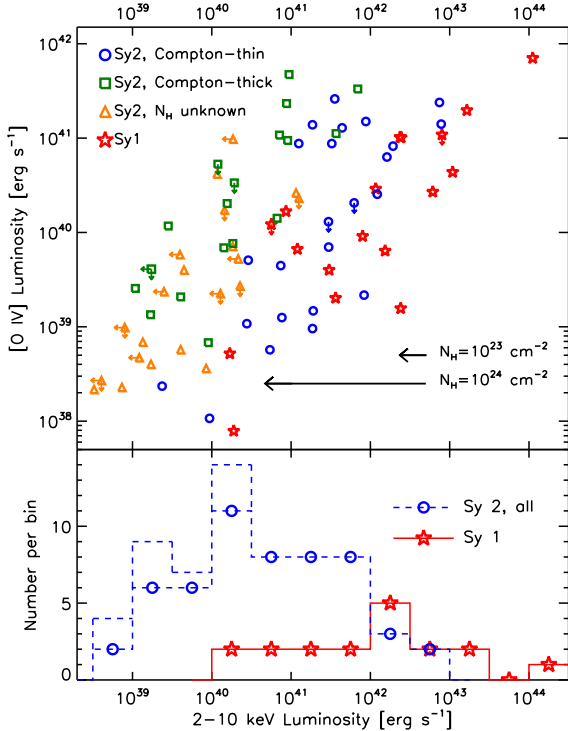


FIG. 4.— Top panel: The relationship between observed $[O\text{ IV}]\lambda 25.89\mu\text{m}$ and 2–10 keV X-ray luminosities. No extinction corrections have been applied. The symbols are as in Figure 2. A clear sequence can be seen between the location of Sy1s, Compton-thin Sy2s, and Compton-thick Sy2s that reflects increasing amounts of X-ray obscuration. The observed 2–10 keV X-ray emission is not a reliable indicator of AGN power for sources with significant obscuration. The arrows indicate the effect of column density $N_H = 10^{23}\text{ cm}^{-2}$ and $N_H = 10^{24}\text{ cm}^{-2}$ on the observed X-ray luminosity. Bottom panel: The distribution of 2–10 keV luminosities, with histogram colors and symbols as in Figure 1. The distributions for Sy1s and Sy2s are statistically different with $p < 1 \times 10^{-5}$. This figure illustrates the strong bias against Sy2 galaxies, and particularly against Compton-thick Sy2s in X-ray-selected AGN samples.

the known Compton-thick sources are biased towards high luminosities; lower-luminosity sources with $N_H > 10^{24}\text{ cm}^{-2}$ likely exist in the “ N_H unknown” category, but have not yet been individually identified as Compton thick. We conclude that $[O\text{ III}]\lambda 5007\text{ \AA}$ is a significantly less reliable quantitative indicator of AGN activity than is $[O\text{ IV}]\lambda 25.89\mu\text{m}$.

We show in Figure 3 and Table 4 that the distributions of radio luminosity density for Sy1s and Sy2s are indistinguishable. This result is not surprising given that radio emission is unaffected by dust. The Sy2s without column density measurements are shown, once again, to be intrinsically weaker on average than the rest of the sample. The only source in the sample that exceeds the canonical radio luminosity threshold for radio-loud AGNs ($L_\nu > 10^{32}\text{ erg s}^{-1}\text{ Hz}^{-1}$; e.g., Miller et al. 1990) is NGC1275, but a handful of objects in Figure 3 have large 6 cm/[O IV] flux ratios that are suggestive of a radio-intermediate classification. Besides NGC1275, which falls beyond the range plotted in Figure 3, the 10 objects with the largest ratios are NGC7213, NGC5128, NGC2639, NGC4594, NGC3031, NGC4579, NGC3079, NGC2655, NGC4168, and NGC4472. With these sources excluded, the scatter in Figure 3 reduces from 0.93 dex to 0.57 dex. While this scatter is large, and ra-

dio selection is biased towards sources that emit a larger fraction of their bolometric luminosity in the radio, we conclude that radio luminosity is an isotropic AGN indicator.

The observed 2–10 keV X-ray luminosities of Sy2s are biased compared to those of Sy1s, and with high statistical significance, $p < 1 \times 10^{-5}$. This behavior can be seen in Figure 4 and Table 5, and is not surprising given that one expects typical Sy2 gas column densities of $10^{22}\text{--}10^{25}\text{ cm}^{-2}$ to absorb 10%–100% of the flux in the 2–10 keV energy range. Only much higher X-ray energies promise to be accurate measures of AGN activity levels, although the most obscured sources will still be affected even at > 20 keV energies (e.g., Meléndez et al. 2008a; Rigby et al. 2009). There is a clear offset in Figure 4 between the points corresponding to Sy1s, Compton-thin Sy2s, and Compton-thick Sy2s as one moves towards smaller observed X-ray luminosities. The objects with unknown column densities fall in between and overlap with the Compton-thin and Compton-thick Sy2s, suggesting that many are highly absorbed and that a significant fraction is likely to be Compton-thick. We note that 8/29 objects in this N_H unknown category have no data in the 2–10 keV range, and thus do not appear in Figure 4, nor are they included in the statistical tests.

4. DISCUSSION

We have found that the Sy1s and Sy2s in the RSA sample have quite similar $[O\text{ IV}]\lambda 25.89\mu\text{m}$ luminosity distributions. In a companion paper, Rigby et al. (2009) compare $[O\text{ IV}]$ luminosity to hard (14–195 keV) X-ray luminosity for the RSA Sy1s, and establish $[O\text{ IV}]$ to be a measure of intrinsic AGN luminosity. Thus our result indicates that the Sy1s and Sy2s in the RSA sample are consistent with being drawn from the same parent distribution of intrinsic luminosity. It also confirms that the RSA sample is one of the least-biased AGN samples known, and is well suited for tests of the unification paradigm and the nature of the obscuring material around AGNs. Furthermore, we find that the observed $[O\text{ III}]\lambda 5007\text{ \AA}$ and 2–10 keV X-ray luminosities are biased indicators of AGN intrinsic luminosity, confirming the results of Meléndez et al. (2008a).

4.1. Implications for X-ray-selected AGN samples

It has been argued from deep X-ray surveys with *Chandra* (e.g., Ueda et al. 2003; Steffen et al. 2003) and *XMM-Newton* (e.g., La Franca et al. 2005) that the obscured AGN fraction decreases with increasing luminosity. Such a trend with observed 2–10 keV X-ray luminosity is also seen in Figure 4. However, we have shown that the $[O\text{ IV}]$ luminosity distributions of obscured and unobscured AGNs in the RSA sample are quite similar. Thus, the trend in Figure 4 is most easily explained as a selection effect due to obscuration of Sy2s in the 2–10 keV band. This effect is quite strong in the RSA sample; while Sy1s constitute only 20% of the whole sample, 9/14 of the sources with observed 2–10 keV luminosities $> 10^{42}\text{ erg s}^{-1}$ and all three of the sources with observed $L_X > 10^{43}\text{ erg s}^{-1}$ are Sy1s. The RSA does not include sources at the bright end of the X-ray luminosity function ($\sim 10^{45}\text{ erg s}^{-1}$) and thus is not able to probe the luminosity dependence of the obscured AGN fraction to the highest luminosities, but the large selection effects at lower luminosity are striking. As suggested by our results for local AGNs, Dwelly & Page (2006) find that the absorption of X-ray sources in the Chandra Deep Field South

is best described by models where the obscured fraction is constant with luminosity, and Treister et al. (2005) also argue that the the observed decrease with luminosity can be explained as a selection effect. Interestingly, a lower incidence of obscured sources at higher luminosities is found by Sazonov et al. (2007) in an all-sky X-ray with INTEGRAL in the 17–60 keV band, which covers $\sim 75\%$ of the sky down to a relatively shallow flux level $f = 7 \times 10^{-11} \text{ erg cm}^{-2} \text{ s}^{-1}$. This result may indicate that even very hard X-rays are biased tracers of obscured AGNs, as suggested by Rigby et al. (2009). If so, then deep surveys with Chandra and XMM-Newton will remain biased up to redshifts of $z \sim 3$ or more, despite their sampling of rest-frame X-ray energies $\geq 20 \text{ keV}$ at these redshifts.

4.2. Possible Missing AGNs

What sources could the RSA sample be missing? The most obvious group of AGNs would be those that lack signs of accretion activity in optical spectra (e.g., Rigby et al. 2006; Ghosh et al. 2008). It is clear from Figure 2 that there are some objects in the RSA with extreme [O IV]/[O III] ratios, but these objects are all at the bright end of the [O IV] flux distribution with $f > 3 \times 10^{-13} \text{ erg cm}^{-2} \text{ s}^{-1}$ and corresponding [O III] fluxes $\sim 10^{-14} \text{ erg cm}^{-2} \text{ s}^{-1}$. It is reasonable to expect that sources with such highly extinguished [O III] would also exist at fainter flux levels, but may be missed by optical emission-line selection. Such selection would also miss any AGN so deeply embedded that the continuum source is not able to photoionize the narrow-line region. This implies that the 4:1 ratio of obscured to unobscured Seyferts in the RSA sample is a lower limit.

We have made a preliminary evaluation of the incidence of “missing” obscured Seyferts from the *Spitzer* spectra of star-forming galaxies in the SINGS sample (Kennicutt et al. 2003) published by Dale et al. (2009). Among the $B_T \leq 13$ RSA galaxies in Dale et al. (2009), 28/51 have $> 2\sigma$ [O IV] detections, but many of these lines are quite weak, especially when compared to [Ne II] $\lambda 12.81 \mu\text{m}$. Except for NGC1705, every galaxy with $[\text{O IV}]/[\text{Ne II}] > 0.05$ (corresponding to $> 2\%$ AGN contribution; Sturm et al. 2002; Armus et al. 2007) is optically classified as an AGN (LINER or Seyfert) by J. Moustakas et al. (2009, in preparation). The remaining candidate, NGC1705, is a dwarf starburst galaxy with an [O IV] luminosity $< 10^{38} \text{ erg s}^{-1}$, smaller than any of the RSA

Seyferts. Ultraviolet spectra of this galaxy show evidence for Wolf-Rayet stars (Meurer et al. 1992) that could explain its observed [O IV]/[Ne II] ratio (e.g., Schaefer & Stasińska 1999). It is also anomalously weak in the radio, even for a star-forming galaxy (Cannon et al. 2006), so we conclude that it is not likely that NGC1705 contains a genuine active nucleus. Thus the incidence of AGNs that are missed by optical emission-line selection does not appear to be large (but see also Satyapal et al. 2008).

5. SUMMARY AND CONCLUSIONS

We have presented measurements of [O IV] $\lambda 25.89 \mu\text{m}$ luminosity for 89 Seyfert galaxies from the RSA sample and compared the distributions of [O IV], [O III] $\lambda 5007 \text{ \AA}$, 2–10 keV X-ray, and 6 cm radio luminosities among Sy1s and Sy2s. We find that the distribution of [O IV] luminosities for Sy2s is indistinguishable from that for Sy1s, while their [O III] luminosity distributions are statistically different. Under the assumption that [O IV] is an accurate tracer of intrinsic AGN luminosity, this indicates that the obscured and unobscured RSA Seyferts are consistent with being drawn from the same parent luminosity distribution, and argues against models where the ratio of obscured to unobscured AGNs depends on luminosity. It also indicates that there is significant extinction towards or within the narrow-line region in a subset of Sy2s. Additionally, we find that obscured and unobscured AGNs have similar distributions of radio luminosities, while their observed X-ray luminosities are quite different, which provides insight into the nature of the sources missed by X-ray surveys.

We acknowledge helpful discussions with Jennifer Donley, Yong Shi, Suresh Sivanadom, Amelia Stutz, Jonathan Trump, and Benjamin Weiner. We thank John Moustakas for providing optical classifications for the SINGS sample in advance of publication and for comments on the manuscript. We also thank Miwa Block for assistance with the reduction of IRS spectral mapping data, Gonzalo Aniano for independent measurements of the [O IV] line fluxes, and the anonymous referee for valuable feedback. This work was partially supported by contract 1255094 from JPL/CalTech to the University of Arizona.

Facilities: Spitzer

REFERENCES

- Antonucci, R. 1993, ARA&A, 31, 473
- Armus, L., et al. 2007, ApJ, 656, 148
- Balmaverde, B., & Capetti, A. 2006, A&A, 447, 97
- Balmaverde, B., Capetti, A., & Grandi, P. 2006, A&A, 451, 35
- Bassani, L., Dadina, M., Maiolino, R., Salvati, M., Risaliti, G., della Ceca, R., Matt, G., & Zamorani, G. 1999, ApJS, 121, 473
- Bianchi, S., Matt, G., Fiore, F., Fabian, A. C., Iwasawa, K., & Nicastro, F. 2002, A&A, 396, 793
- Bianchi, S., Matt, G., Balestra, I., Guainazzi, M., & Perola, G. C. 2004, A&A, 422, 65
- Bianchi, S., Guainazzi, M., & Chiaberge, M. 2006, A&A, 448, 499
- Bianchi, S., Corral, A., Panessa, F., Barcons, X., Matt, G., Bassani, L., Carrera, F. J., & Jiménez-Bailón, E. 2008, MNRAS, 385, 195
- Bansford, M. A., Appleton, P. N., Heisler, C. A., Norris, R. P., & Marston, A. P. 1998, ApJ, 497, 133
- Brightman, M., & Nandra, K. 2008, MNRAS, 390, 1241
- Cappi, M., et al. 2006, A&A, 446, 459
- Cannon, J. M., et al. 2006, ApJ, 647, 293
- Chiaberge, M., Gilli, R., Macchetto, F. D., & Sparks, W. B. 2006, ApJ, 651, 728
- Condon, J. J., Cotton, W. D., Greisen, E. W., Yin, Q. F., Perley, R. A., Taylor, G. B., & Broderick, J. J. 1998, AJ, 115, 1693
- Cruz-Gonzalez, I., Carrasco, L., Serrano, A., Guichard, J., Dultzin-Hacyan, D., & Bisiacchi, G. F. 1994, ApJS, 94, 47
- Dadina, M. 2007, A&A, 461, 1209
- Dale, D. A., et al. 2009, ApJ, 693, 1821
- Davies, R. E., et al. 1998, MNRAS, 293, 189
- Done, C., Madejski, G. M., & Smith, D. A. 1996, ApJ, 463, L63
- Dong, H., Xue, S.-J., Li, C., & Cheng, F.-Z. 2004, Chin. J. Astron. Astrophys., 4, 427
- Dwelly, T., & Page, M. J. 2006, MNRAS, 372, 1755
- Evans, D. A., Worrall, D. M., Hardcastle, M. J., Kraft, R. P., & Birkinshaw, M. 2006, ApJ, 642, 96
- de Grijp, M. H. K., Keel, W. C., Miley, G. K., Goudfrooij, P., & Lub, J. 1992, A&AS, 96, 389
- Feigelson, E. D., & Nelson, P. I. 1985, ApJ, 293, 192
- Feldmeier, J. J., Ciardullo, R., & Jacoby, G. H. 1997, ApJ, 479, 231
- Freedman, W. L., et al. 2001, ApJ, 553, 47
- Fricke, K. J., & Kollatschny, W. 1989, A&AS, 77, 75
- Fukazawa, Y., Iyomoto, N., Kubota, A., Matsumoto, Y., & Makishima, K. 2001, A&A, 374, 73
- Ghosh, H., Mathur, S., Fiore, F., & Ferrarese, L. 2008, ApJ, 687, 216
- Gilli, R., Maiolino, R., Marconi, A., Risaliti, G., Dadina, M., Weaver, K. A., & Colbert, E. J. M. 2000, A&A, 355, 485
- Grandi, P., et al. 2003, ApJ, 593, 160

- Gu, Q., Melnick, J., Fernandes, R. C., Kunth, D., Terlevich, E., & Terlevich, R. 2006, MNRAS, 366, 480
- Guainazzi, M. 2002, MNRAS, 329, L13
- Guainazzi, M., Matt, G., & Perola, G. C. 2005, A&A, 444, 119
- Guainazzi, M., Fabian, A. C., Iwasawa, K., Matt, G., & Fiore, F. 2005, MNRAS, 356, 295
- Haas, M., Siebenmorgen, R., Schulz, B., Krügel, E., & Chini, R. 2005, A&A, 442, L39
- Ho, L. C., Filippenko, A. V., & Sargent, W. L. 1995, ApJS, 98, 477
- Ho, L. C., Filippenko, A. V., & Sargent, W. L. W. 1997, ApJS, 112, 315
- Ho, L. C., Ptak, A., Terashima, Y., Kunieda, H., Serlemitsos, P. J., Yaqoob, T., & Koratkar, A. P. 1999, ApJ, 525, 168
- Ho, L. C., & Ulvestad, J. S. 2001, ApJS, 133, 77
- Houck, J. R., et al. 2004, ApJS, 154, 18
- Iwasawa, K., Maloney, P. R., & Fabian, A. C. 2002, MNRAS, 336, L71
- Iwasawa, K., Wilson, A. S., Fabian, A. C., & Young, A. J. 2003, MNRAS, 345, 369
- Iyomoto, N., Fukazawa, Y., Nakai, N., & Ishihara, Y. 2001, ApJ, 561, L69
- Jones, P. A., McAdam, W. B., & Reynolds, J. E. 1994, MNRAS, 268, 602
- Karachentsev, I. D., et al. 2003, A&A, 398, 467
- Kaspi, S., et al. 2001, ApJ, 554, 216
- Kennicutt, R. C., Jr., et al. 2003, PASP, 115, 928
- Kewley, L. J., Heisler, C. A., Dopita, M. A., Sutherland, R., Norris, R. P., Reynolds, J., & Lumsden, S. 2000, ApJ, 530, 704
- Laor, A. 2003, ApJ, 590, 86
- Lavalley, M., Isobe, T., & Feigelson, E. 1992, in ASP Conf. Ser. 25, Astronomical Data Analysis Software and Systems I, ed. D. M. Worrall, C. Biemesderfer, & J. Barnes (San Francisco, CA: ASP), 245
- Levenson, N. A., Weaver, K. A., & Heckman, T. M. 2001, ApJS, 133, 269
- Levenson, N. A., Weaver, K. A., Heckman, T. M., Awaki, H., & Terashima, Y. 2004, ApJ, 602, 135
- Levenson, N. A., Weaver, K. A., Heckman, T. M., Awaki, H., & Terashima, Y. 2005, ApJ, 618, 167
- Levenson, N. A., Heckman, T. M., Krolik, J. H., Weaver, K. A., & Źycki, P. T. 2006, ApJ, 648, 111
- La Franca, F., et al. 2005, ApJ, 635, 864
- Lawrence, A. 1991, MNRAS, 252, 586
- Maiolino, R., & Rieke, G. H. 1995, ApJ, 454, 95
- Maiolino, R., Salvati, M., Bassani, L., Dadina, M., della Ceca, R., Matt, G., Risaliti, G., & Zamorani, G. 1998, A&A, 338, 781
- Matt, G., Fabian, A. C., Guainazzi, M., Iwasawa, K., Bassani, L., & Malagutti, G. 2000, MNRAS, 318, 173
- McKernan, B., Yaqoob, T., & Reynolds, C. S. 2007, MNRAS, 379, 1359
- Meléndez, M., et al. 2008, ApJ, 682, 94
- Meléndez, M., Kraemer, S. B., Schmitt, H. R., Crenshaw, D. M., Deo, R. P., Mushotzky, R. F., & Bruhweiler, F. C. 2008, ApJ, 689, 95
- Meurer, G. R., Freeman, K. C., Dopita, M. A., & Cacciari, C. 1992, AJ, 103, 60
- Miller, L., Peacock, J. A., & Mead, A. R. G. 1990, MNRAS, 244, 207
- Moran, E. C., Eracleous, M., Leighly, K. M., Chartas, G., Filippenko, A. V., Ho, L. C., & Blanco, P. R. 2005, AJ, 129, 2108
- Morganti, R., Tsvetanov, Z. I., Gallimore, J., & Allen, M. G. 1999, A&AS, 137, 457
- Mould, J. R., et al. 2000, ApJ, 529, 786
- Neff, S. G., & Hutchings, J. B. 1992, AJ, 103, 1746
- Nemmen, R. S., Storchi-Bergmann, T., Yuan, F., Eracleous, M., Terashima, Y., & Wilson, A. S. 2006, ApJ, 643, 652
- Netzer, H., Chelouche, D., George, I. M., Turner, T. J., Crenshaw, D. M., Kraemer, S. B., & Nandra, K. 2002, ApJ, 571, 256
- Nicastro, F., Martocchia, A., & Matt, G. 2003, ApJ, 589, L13
- Oliva, E., Salvati, M., Moorwood, A. F. M., & Marconi, A. 1994, A&A, 288, 457
- Pappa, A., Georgantopoulos, I., Stewart, G. C., & Zezas, A. L. 2001, MNRAS, 326, 995
- Pellegrini, S., Fabbiano, G., Fiore, F., Trinchieri, G., & Antonelli, A. 2002, A&A, 383, 1
- Reynolds, C. S. 1997, MNRAS, 286, 513
- Rigby, J. R., Rieke, G. H., Donley, J. L., Alonso-Herrero, A., & Pérez-González, P. G. 2006, ApJ, 645, 115
- Rigby, J. R., Diamond-Stanic, A. M., & Aniano, G. 2009, ApJ in press, arXiv:0905.2956
- Risaliti, G. 2002, A&A, 386, 379
- Risaliti, G., Elvis, M., Fabbiano, G., Baldi, A., & Zezas, A. 2005, ApJ, 623, L93
- Sadler, E. M., Slee, O. B., Reynolds, J. E., & Roy, A. L. 1995, MNRAS, 276, 1373
- Salvati, M., Bassani, L., della Ceca, R., Maiolino, R., Matt, G., & Zamorani, G. 1997, A&A, 323, L1
- Sandage, A., & Tammann, G. A. 1987, A Revised Shapley–Ames Catalog of Bright Galaxies (2nd ed. Washington, DC: Carnegie Institution of Washington)
- Sandqvist, A., Joersaeter, S., & Lindblad, P. O. 1995, A&A, 295, 585
- Satyapal, S., Vega, D., Dudik, R. P., Abel, N. P., & Heckman, T. 2008, ApJ, 677, 926
- Saxton, R. D., Read, A. M., Esquej, P., Freyberg, M. J., Altieri, B., & Bermejo, D. 2008, A&A, 480, 611
- Sazonov, S., Revnivtsev, M., Krivonos, R., Churazov, E., & Sunyaev, R. 2007, A&A, 462, 57
- Schaerer, D., & Stasińska, G. 1999, A&A, 345, L17
- Schmitt, H. R., Ulvestad, J. S., Antonucci, R. R. J., & Kinney, A. L. 2001, ApJS, 132, 199
- Schönnauer, R. A., Caldwell, N., Wilson, A. S., Baldwin, J. A., Phillips, M. M., Williams, T. B., & Turtle, A. J. 1988, ApJ, 324, 154
- Shapley, H., & Ames, A. 1932, Ann. Harvard College Obs., 88, 41
- Slee, O. B., Sadler, E. M., Reynolds, J. E., & Ekers, R. D. 1994, MNRAS, 269, 928
- Smith, J. D. T., et al. 2007, PASP, 119, 1133
- Spoon, H. W. W., Koornneef, J., Moorwood, A. F. M., Lutz, D., & Tielens, A. G. M. 2000, A&A, 357, 898
- Stauffer, J. R. 1982, ApJ, 262, 66
- Steffen, A. T., Barger, A. J., Cowie, L. L., Mushotzky, R. F., & Yang, Y. 2003, ApJ, 596, L23
- Steenbrugge, K. C., et al. 2003, A&A, 408, 921
- Sturm, E., Lutz, D., Verma, A., Netzer, H., Sternberg, A., Moorwood, A. F. M., Oliva, E., & Genzel, R. 2002, A&A, 393, 821
- Terashima, Y., Kunieda, H., & Misaki, K. 1999, PASJ, 51, 277
- Terashima, Y., Iyomoto, N., Ho, L. C., & Ptak, A. F. 2002, ApJS, 139, 1
- Thean, A., Pedlar, A., Kukula, M. J., Baum, S. A., & O’Dea, C. P. 2000, MNRAS, 314, 573
- Tran, H. D. 2003, ApJ, 583, 632
- Treister, E., et al. 2005, ApJ, 621, 104
- Turner, T. J., George, I. M., Nandra, K., & Mushotzky, R. F. 1997, ApJS, 113, 23
- Turner, T. J., Nandra, K., Turcan, D., & George, I. M. 2001, in AIP Conf. Proc. 599, X-ray Astronomy: Stellar Endpoints, AGN, and the Diffuse X-ray Background, ed. N. E. White, G. Malagutti, & G. G. C. Palumbo (Melville, NY: AIP), 991
- Ueda, Y., Akiyama, M., Ohta, K., & Miyaji, T. 2003, ApJ, 598, 886
- Ulvestad, J. S., & Wilson, A. S. 1984, ApJ, 285, 439
- Ulvestad, J. S., & Wilson, A. S. 1989, ApJ, 343, 659
- Vaceli, M. S., Viegas, S. M., Gruenwald, R., & de Souza, R. E. 1997, AJ, 114, 1345
- Veron-Cetty, M.-P., & Veron, P. 1986, A&AS, 66, 335
- Vignali, C., & Comastri, A. 2002, A&A, 381, 834
- Vila, M. B., Pedlar, A., Davies, R. D., Hummel, E., & Axon, D. J. 1990, MNRAS, 242, 379
- Watson, M. G., et al. 2009, A&A, 493, 339
- Werner, M. W., et al. 2004, ApJS, 154, 1
- White, R. L., Becker, R. H., Helfand, D. J., & Gregg, M. D. 1997, ApJ, 475, 479
- Winkler, H. 1992, MNRAS, 257, 677
- Yang, Y., Wilson, A. S., & Ferruit, P. 2001, ApJ, 563, 124
- Yang, Y., Li, B., Wilson, A. S., & Reynolds, C. S. 2007, ApJ, 660, 1106
- Yaqoob, T., McKernan, B., Kraemer, S. B., Crenshaw, D. M., Gabel, J. R., George, I. M., & Turner, T. J. 2003, ApJ, 582, 105
- Yaqoob, T., & Padmanabhan, U. 2004, ApJ, 604, 63
- Young, A. J., Wilson, A. S., & Shopbell, P. L. 2001, ApJ, 556, 6
- Zhang, J. S., Henkel, C., Kadler, M., Greenhill, L. J., Nagar, N., Wilson, A. S., & Braatz, J. A. 2006, A&A, 450, 933

AGN Luminosity Indicators

TABLE 1
TABLE OF MEASUREMENTS

| NAME (1) | D (2) | Seyfert Type (3) | [O IV] (4) | σ (5) | [O III] (6) | Ref (7) | 6 cm (8) | Ref (9) | 2 – 10 keV (10) | N_H (11) | Ref (12) |
|----------------|------------------|------------------------|-----------------------|-----------------|----------------|------------|-------------|------------|--------------------|---------------|-------------|
| NGC777 | 66.5 | 2 | <4.35e-14 | 1.45e-14 | <2.4e-15 | 1 | 1.4e-26 | 11 | 2.4e-13 | ... | 29 |
| NGC788 | 54.1 | 2 | 1.80e-13 | 0.08e-13 | 3.6e-14 | 2 | 1.2e-26 | 12 | 4.6e-12 | 3.0e+23 | 30 |
| NGC1068 | 14.4 | 1.8 | 1.90e-11 ^d | 0.19e-11 | 3.6e-12 | 2 | 5.2e-24 | 11 | 3.8e-12 | >1.0e+25 | 31,32 |
| NGC1058 | 9.2 ^a | 2 | <2.66e-14 | 0.69e-14 | 1.4e-15 | 1 | <1.2e-27 | 11 | <4.0e-14 | ... | 33 |
| NGC1097 | 16.5 | 1.0 | <3.74e-13 | 0.57e-13 | 1.5e-14 | 3 | 3.8e-26 | 13 | 1.7e-12 | 2.3e+20 | 34 |
| NGC1241 | 53.8 | 2 | <1.40e-13 | 0.16e-13 | 1.6e-15 | 4 | 1.0e-25 | 14 | ... | ... | |
| NGC1275 | 70.1 | 1.5 | <1.85e-13 | 0.40e-13 | 6.9e-13 | 1 | 2.1e-22 | 11 | 1.4e-11 | <1.5e+21 | 35,36 |
| NGC1365 | 21.5 | 1.8 | 1.58e-12 | 0.12e-12 | 6.2e-14 | 3 | 9.0e-27 | 15 | 5.9e-12 | 4.0e+23 | 37 |
| NGC1358 | 53.6 | 2 | 7.61e-14 | 1.43e-14 | 2.0e-13 | 1 | 1.2e-26 | 11 | 3.4e-13 | ... | 30 |
| NGC1386 | 10.6 | 2 | 8.70e-13 | 0.27e-13 | 2.7e-13 | 3 | 1.3e-25 | 16 | 2.1e-13 | >1.0e+24 | 38 |
| NGC1433 | 13.3 | 2 | 6.07e-14 | 1.12e-14 | 2.1e-14 | 3 | <3.0e-26 | 16 | ... | ... | |
| NGC1566 | 19.4 | 1.5 | 8.88e-14 | 0.46e-14 | 1.7e-13 | 3 | <6.0e-26 | 16 | 6.7e-12 | ... | 39 |
| NGC1667 | 61.2 | 2 | 9.28e-14 | 1.48e-14 | 9.1e-15 | 2 | 1.2e-26 | 11 | 2.6e-14 | ... | 40 |
| NGC2273 | 28.4 | 2 | 1.47e-13 | 0.20e-13 | 2.8e-13 | 1 | 1.4e-25 | 11 | 6.9e-13 | >1.8e+24 | 41 |
| NGC2639 | 42.6 | 1.9 | 3.27e-14 | 0.38e-14 | 1.9e-14 | 1 | 1.7e-24 | 11 | 8.5e-14 | ... | 30 |
| NGC2685 | 16.2 | 2 | 1.15e-14 | 0.35e-14 | 8.1e-15 | 1 | <1.3e-27 | 11 | 2.7e-13 | ... | 33 |
| NGC2655 | 24.4 | 2 | 6.25e-14 | 1.41e-14 | 3.9e-14 | 1 | 3.4e-25 | 11 | 1.0e-12 | 4.5e+23 | 42 |
| NGC2992 | 34.1 | 1.9 | 1.08e-12 | 0.03e-12 | 5.2e-14 | 2 | 7.0e-26 | 16 | 6.3e-12 | 1.4e+22 | 43 |
| NGC3031 | 3.6 ^a | 1.5 | 4.99e-14 | 0.94e-14 | 2.2e-13 | 1 | 8.4e-25 | 11 | 1.2e-11 | 1.0e+21 | 33 |
| NGC3081 | 34.2 | 2 | 9.89e-13 | 0.20e-13 | 2.1e-13 | 2 | 9.0e-27 | 12 | 1.3e-12 | 6.4e+23 | 44 |
| NGC3079 | 20.4 | 2 | 1.53e-13 | 0.38e-13 | 1.8e-15 | 1 | 9.2e-25 | 11 | 3.7e-13 | >1.0e+25 | 45 |
| IC2560 | 40.7 | 2 | 5.43e-13 | 0.17e-13 | 1.3e-13 | 2 | 9.5e-26 | 13 | 3.6e-13 | >1.0e+24 | 46,41 |
| NGC3147 | 40.9 | 2 | <6.50e-14 | 1.35e-14 | 1.7e-14 | 1 | 1.0e-25 | 11 | 1.5e-12 | <1.7e+22 | 47,48 |
| NGC3185 | 21.3 | 2 | 4.70e-14 | 1.62e-14 | 5.0e-14 | 1 | 1.9e-27 | 11 | 2.0e-14 | >1.0e+24 | 33 |
| NGC3227 | 20.6 | 1.5 | 5.71e-13 | 0.45e-13 | 9.4e-13 | 1 | 2.0e-25 | 11 | 2.3e-11 | 1.9e+22 | 49,50 |
| NGC3254 | 23.6 | 2 | <1.47e-14 | 0.45e-14 | 6.0e-15 | 1 | <1.2e-27 | 11 | <1.2e-14 | ... | 29 |
| NGC3281 | 44.7 | 2 | 1.39e-12 | 0.04e-12 | 1.3e-14 | 2 | 2.7e-25 | 12 | 2.9e-12 | 1.5e+24 | 51 |
| NGC3486 | 7.4 | 2 | 3.30e-14 | 1.16e-14 | 1.3e-14 | 1 | <1.2e-27 | 11 | 5.0e-14 | ... | 52 |
| NGC3516 | 38.9 | 1.2 | 5.60e-13 | 0.23e-13 | 3.5e-13 | 1 | 3.2e-26 | 11 | 1.4e-11 | 7.9e+21 | 53 |
| IRAS11215-2806 | 62.4 | 2 | 9.97e-14 | 0.64e-14 | 5.1e-14 | 5 | 1.8e-25 | 17 | ... | ... | |
| NGC3735 | 41.0 | 2 | 4.84e-13 | 0.18e-13 | 3.7e-14 | 1 | 8.1e-27 | 11 | <9.2e-14 | ... | 29 |
| NGC3783 | 36.1 | 1.2 | 2.80e-13 | 0.25e-13 | 8.3e-13 | 6 | 1.3e-25 | 16 | 7.0e-11 | 8.7e+21 | 30,54 |
| NGC3941 | 18.9 | 2 | 9.35e-15 | 4.59e-15 | 7.7e-15 | 1 | 2.3e-27 | 11 | 4.0e-14 | ... | 33 |
| NGC3976 | 37.7 | 2 | <1.01e-13 | 0.20e-13 | 7.7e-15 | 1 | 4.5e-27 | 11 | 8.5e-14 | ... | 29 |
| NGC3982 | 17.0 | 1.9 | <1.18e-13 | 0.16e-13 | 2.0e-13 | 1 | 1.8e-26 | 11 | <5.0e-14 | >1.6e+24 | 55 |
| NGC4051 | 17.0 | 1.2 | 2.64e-13 | 0.25e-13 | 4.4e-13 | 1 | 2.1e-26 | 11 | 2.3e-11 | <2.8e+21 | 30,47 |
| NGC4138 | 17.0 | 1.9 | 4.27e-14 | 0.32e-14 | 1.6e-14 | 1 | 7.8e-27 | 11 | 5.5e-12 | 8.0e+22 | 33 |
| NGC4151 | 20.3 | 1.5 | 2.08e-12 | 0.08e-12 | 1.1e-11 | 1 | 8.1e-25 | 11 | 4.8e-11 | 3.1e+22 | 56 |
| NGC4168 | 16.8 | 1.9 | 1.39e-14 | 0.44e-14 | 2.4e-15 | 1 | 5.0e-26 | 11 | <3.6e-14 | ... | 57 |
| NGC4235 | 35.1 | 1.2 | 4.33e-14 | 0.78e-14 | 2.0e-14 | 1 | 5.1e-26 | 11 | 1.0e-11 | 3.0e+21 | 30 |
| NGC4258 | 8.0 ^a | 1.9 | 7.49e-14 | 1.23e-14 | 1.0e-13 | 1 | 1.8e-26 | 11 | 7.1e-12 | 8.2e+22 | 58 |
| NGC4378 | 35.1 | 2 | <1.83e-14 | 0.61e-14 | 5.0e-15 | 1 | 3.0e-27 | 11 | 1.5e-13 | ... | 29 |
| NGC4388 | 16.8 | 1.9 | 2.59e-12 | 0.03e-12 | 1.6e-13 | 2 | 5.4e-26 | 11 | 3.7e-12 | 3.5e+23 | 59 |
| NGC4395 | 4.6 ^b | 1.8 | 4.23e-14 | 0.31e-14 | 1.4e-13 | 1 | 6.8e-27 | 11 | 3.7e-12 | 1.2e+22 | 60 |
| NGC4472 | 16.8 | 2 | <6.64e-14 | 1.89e-14 | 1.9e-15 | 1 | 1.9e-25 | 11 | <3.8e-13 | ... | 33 |
| NGC4477 | 16.8 | 2 | 1.69e-14 | 0.56e-14 | 1.9e-14 | 1 | 1.7e-27 | 11 | 1.2e-13 | ... | 33 |
| NGC4501 | 16.8 | 2 | 3.98e-14 | 0.34e-14 | 3.7e-14 | 1 | 1.1e-26 | 11 | 5.0e-14 | >1.0e+24 | 61 |
| NGC4507 | 59.6 | 2 | 3.31e-13 | 0.22e-13 | 4.5e-13 | 2 | 1.1e-25 | 18 | 1.8e-11 | 5.9e+23 | 62 |
| NGC4565 | 9.7 | 1.9 | 2.09e-14 | 1.52e-14 | 1.5e-14 | 1 | 2.6e-26 | 11 | 2.1e-13 | 2.5e+21 | 63 |
| NGC4579 | 16.8 | 1.9 | 2.83e-14 | 0.62e-14 | 7.8e-14 | 1 | 3.8e-25 | 11 | 5.5e-12 | 3.3e+21 | 48 |
| NGC4593 | 41.3 | 1.0 | 1.32e-13 | 0.27e-13 | 1.3e-13 | 5 | 1.6e-26 | 19 | 3.0e-11 | 1.6e+21 | 64 |
| NGC4594 | 20.0 | 1.9 | 2.62e-14 | 0.43e-14 | 4.7e-14 | 1 | 1.2e-24 | 16 | 1.6e-12 | 1.7e+21 | 65 |
| IC3639 | 35.3 | 2 | <3.55e-13 | 0.73e-13 | 4.1e-13 | 4 | 2.0e-25 | 16 | 8.0e-14 | >1.6e+24 | 54 |
| NGC4639 | 16.8 | 1.0 | 1.54e-14 | 0.43e-14 | 7.5e-15 | 1 | 2.2e-27 | 11 | 5.0e-13 | 7.3e+20 | 66 |
| NGC4698 | 16.8 | 2 | 2.03e-14 | 0.37e-14 | 1.9e-14 | 1 | 2.6e-27 | 11 | 4.0e-14 | ... | 33 |
| NGC4725 | 12.4 | 2 | 1.24e-14 | 0.31e-14 | 2.0e-14 | 1 | <1.7e-27 | 11 | 4.0e-14 | ... | 33 |
| NGC4941 | 16.8 | 2 | 1.50e-13 | 0.18e-13 | 1.4e-13 | 2 | 4.3e-26 | 12 | 8.5e-13 | 6.9e+23 | 67 |
| NGC4939 | 46.6 | 2 | 4.30e-13 | 0.08e-13 | 1.6e-13 | 2 | 7.0e-27 | 20 | 1.4e-12 | >1.0e+25 | 44 |
| NGC4945 | 4.3 | 2 | 3.00e-13 ^e | 0.60e-13 | ... | 2 | 2.9e-25 | 21 | 4.0e-12 | 5.0e+24 | 30,68 |
| NGC5005 | 21.3 | 2 | 1.99e-14 | 1.44e-14 | 4.7e-14 | 1 | 2.7e-26 | 20 | 5.1e-13 | 3.0e+22 | 41 |
| NGC5033 | 18.7 | 1.5 | 1.59e-13 | 0.07e-13 | 5.3e-14 | 1 | 3.0e-26 | 11 | 2.9e-12 | <8.7e+20 | 33,69 |
| NGC5128 | 4.3 | 2 | 9.89e-13 | 0.79e-13 | 1.2e-14 | 3 | 7.0e-23 | 22 | 3.8e-10 | 1.0e+23 | 70 |
| NGC5135 | 57.7 | 2 | 5.83e-13 | 0.34e-13 | 3.6e-14 | 2 | 5.9e-25 | 12 | 2.2e-13 | >1.0e+24 | 71 |
| NGC5194 | 8.4 ^c | 2 | 2.46e-13 | 0.10e-13 | 1.1e-13 | 1 | 9.8e-27 | 11 | 4.8e-13 | 5.6e+24 | 33,72 |
| NGC5273 | 21.3 | 1.5 | 3.72e-14 | 1.42e-14 | 1.2e-13 | 1 | 1.0e-26 | 11 | 6.7e-12 | 9.0e+21 | 33 |
| NGC5395 | 46.7 | 2 | <9.29e-14 | 1.77e-14 | 1.8e-15 | 1 | 1.9e-27 | 11 | ... | ... | |
| NGC5427 | 40.4 | 2 | 2.68e-14 | 0.58e-14 | 5.5e-14 | 2 | 2.5e-26 | 13 | <1.1e-13 | ... | 54 |
| CIRCINUS | 2.9 | 2 | 6.79e-12 ^d | 1.36e-12 | 8.3e-14 | 7 | 3.4e-25 | 23 | 1.4e-11 | 4.0e+24 | 73 |
| NGC5506 | 30.0 | 1.9 | 2.22e-12 | 0.07e-12 | 1.6e-13 | 2 | 1.6e-24 | 16 | 6.9e-11 | 3.2e+22 | 74 |
| NGC5631 | 32.7 | 2 | 1.46e-14 | 0.39e-14 | 4.5e-15 | 1 | 3.7e-27 | 11 | ... | ... | |
| NGC5643 | 14.4 | 2 | 8.16e-13 | 0.41e-13 | 2.4e-13 | 2 | 1.6e-26 | 24 | 6.3e-13 | >1.0e+24 | 75 |
| NGC5728 | 41.1 | 2 | 1.29e-12 | 0.02e-12 | 1.2e-13 | 2 | 5.2e-26 | 25 | 1.8e-12 | 8.2e+23 | 76 |
| NGC5899 | 42.8 | 2 | 2.63e-13 | 0.15e-13 | 6.9e-14 | 8 | 4.0e-26 | 26 | ... | ... | |

TABLE 1
TABLE OF MEASUREMENTS

| | | | | | | | | | | | |
|---------|-------|-----|-----------|----------|---------|----|----------|----|----------|----------|----|
| NGC6221 | 19.3 | 2 | <4.62e-13 | 0.90e-13 | 2.5e-14 | 2 | <1.0e-26 | 16 | 1.4e-11 | 1.0e+22 | 77 |
| NGC6300 | 14.0 | 2 | 2.98e-13 | 0.47e-13 | 2.3e-14 | 2 | 4.2e-26 | 13 | 1.3e-11 | 2.1e+23 | 78 |
| NGC6814 | 25.6 | 1.5 | 2.13e-13 | 0.21e-13 | 7.0e-14 | 6 | 2.0e-26 | 16 | 1.1e-12 | <5.8e+20 | 79 |
| NGC6951 | 24.1 | 2 | 8.37e-14 | 2.01e-14 | 7.0e-15 | 1 | 1.0e-26 | 11 | <5.7e-14 | ... | 29 |
| MRK509 | 143.8 | 1.2 | 2.85e-13 | 0.11e-13 | 8.6e-13 | 9 | 1.8e-26 | 27 | 4.5e-11 | 2.1e+21 | 80 |
| NGC7130 | 68.7 | 2 | 1.67e-13 | 0.34e-13 | 1.1e-13 | 2 | 3.8e-25 | 16 | 1.6e-13 | >1.0e+24 | 81 |
| NGC7172 | 37.6 | 2 | 4.86e-13 | 0.15e-13 | 1.3e-14 | 2 | 1.2e-25 | 13 | 1.1e-11 | 1.1e+23 | 48 |
| NGC7213 | 24.9 | 1.5 | 2.11e-14 | 1.21e-14 | 3.4e-13 | 6 | 2.1e-24 | 18 | 3.3e-11 | <4.2e+21 | 48 |
| NGC7314 | 20.8 | 1.9 | 4.91e-13 | 0.12e-13 | 2.2e-14 | 2 | 2.7e-26 | 13 | 2.4e-11 | 9.3e+21 | 48 |
| NGC7410 | 24.8 | 2 | 4.63e-14 | 1.12e-14 | 1.9e-14 | 4 | 1.4e-26 | 28 | ... | ... | |
| NGC7469 | 67.0 | 1.2 | 3.67e-13 | 0.86e-13 | 5.9e-13 | 10 | 2.1e-25 | 16 | 3.1e-11 | 1.3e+20 | 30 |
| NGC7479 | 32.4 | 1.9 | <2.67e-13 | 0.62e-13 | 1.1e-14 | 1 | 2.7e-26 | 11 | 1.5e-13 | >1.0e+24 | 29 |
| NGC7496 | 23.1 | 2 | <1.87e-13 | 0.48e-13 | 9.6e-15 | 2 | 5.8e-26 | 14 | ... | ... | |
| NGC7582 | 22.0 | 2 | 2.22e-12 | 0.16e-12 | 5.7e-14 | 2 | 6.9e-25 | 16 | 7.6e-12 | 2.3e+23 | 82 |
| NGC7590 | 22.0 | 2 | 6.88e-14 | 1.22e-14 | 1.1e-14 | 2 | <3.0e-27 | 14 | 7.7e-14 | ... | 29 |
| NGC7743 | 24.4 | 2 | 3.30e-14 | 1.79e-14 | 7.9e-15 | 2 | 2.8e-26 | 11 | <3.5e-14 | ... | 29 |

NOTE. — References: (1) Ho et al. (1997). (2) Gu et al. (2006). (3) Veron-Cetty & Veron (1986). (4) Vaceli et al. (1997). (5) de Grijp et al. (1992). (6) Winkler (1992). (7) Oliva et al. (1994). (8) Stauffer (1982). (9) Cruz-Gonzalez et al. (1994). (10) Fricke & Kollatschny (1989). (11) Ho & Ulvestad (2001). (12) Ulvestad & Wilson (1989). (13) Morganti et al. (1999). (14) Thean et al. (2000). (15) Sandqvist et al. (1995). (16) Sadler et al. (1995). (17) Schmitt et al. (2001). (18) Bransford et al. (1998). (19) Ulvestad & Wilson (1984). (20) Vila et al. (1990). (21) Jones et al. (1994). (22) Slep et al. (1994). (23) Davies et al. (1998). (24) Kewley et al. (2000). (25) Schommer et al. (1988). (26) White et al. (1997). (27) Neff & Hutchings (1992). (28) Condon et al. (1998). (29) This work. (30) Turner et al. (2001). (31) Young et al. (2001). (32) Matt et al. (2000). (33) Cappi et al. (2006). (34) Nemmen et al. (2006). (35) Evans et al. (2006). (36) Balmaverde et al. (2006). (37) Risaliti et al. (2005). (38) Levenson et al. (2006). (39) Saxton et al. (2008). (40) Turner et al. (1997). (41) Guainazzi et al. (2005b). (42) Terashima et al. (2002). (43) Gilli et al. (2000). (44) Maiolino et al. (1998). (45) Iyomoto et al. (2001). (46) Iwasawa et al. (2002). (47) Bianchi et al. (2008). (48) Dadina (2007). (49) Yaqoob & Padmanabhan (2004). (50) McKernan et al. (2007). (51) Vignali & Comastri (2002). (52) Pappa et al. (2001). (53) Netzer et al. (2002). (54) Kaspi et al. (2001). (55) Guainazzi et al. (2005a). (56) Yang et al. (2001). (57) Balmaverde & Capetti (2006). (58) Yang et al. (2007). (59) Iwasawa et al. (2003). (60) Moran et al. (2005). (61) Brightman & Nandra (2008). (62) Risaliti (2002). (63) Chiaberge et al. (2006). (64) Steenbrugge et al. (2003). (65) Pellegrini et al. (2002). (66) Ho et al. (1999). (67) Salvati et al. (1997). (68) Done et al. (1996). (69) Terashima et al. (1999). (70) Grandi et al. (2003). (71) Levenson et al. (2004). (72) Fukazawa et al. (2001). (73) Bianchi et al. (2002). (74) Bianchi et al. (2004). (75) Bianchi et al. (2006). (76) Zhang et al. (2006). (77) Levenson et al. (2001). (78) Guainazzi (2002). (79) Reynolds (1997). (80) Yaqoob et al. (2003). (81) Levenson et al. (2005). (82) Dong et al. (2004).

^a Cepheid distance from Freedman et al. (2001).

^b Tip of the red giant branch distance from Karachentsev et al. (2003).

^c Planetary nebula luminosity function distance from Feldmeier et al. (1997).

^d Flux from Sturm et al. (2002). A 20% calibration uncertainty is adopted.

^e Flux from Spoon et al. (2000). A 20% calibration uncertainty is adopted.

TABLE 2
[O IV] STATISTICAL TESTS

| Sy1 v. (1) | Sy2 (2) | Sy2, Compton-thin (3) | Sy2, Compton-thick (4) | Sy2, N_H unknown (5) |
|------------------------------------|------------|--------------------------|---------------------------|---------------------------|
| Gehan, permutation ^a | 0.322 | 0.979 | 0.680 | 0.010 |
| Gehan, hypergeometric ^b | 0.309 | 0.979 | 0.682 | 0.007 |
| logrank ^c | 0.464 | 0.960 | 0.570 | 0.040 |
| Peto-Peto ^d | 0.289 | 0.963 | 0.693 | 0.010 |
| Peto-Prentice ^e | 0.298 | 0.966 | 0.696 | 0.009 |

NOTE. — Col. (1): Seyfert types 1.0–1.5. 18 objects, 2 upper limits. Col. (2): Seyfert types 1.8–2. 71 objects, 14 upper limits. Col. (3): Seyfert types 1.8–2, $N_H < 1 \times 10^{-24} \text{ cm}^{-2}$. 24 objects, 2 upper limits. Col. (4): Seyfert types 1.8–2, $N_H > 1 \times 10^{-24} \text{ cm}^{-2}$. 18 objects, 3 upper limits. Col. (5): Seyfert types 1.8–2, N_H unknown. 29 objects, 9 upper limits. The values in Columns 2–5 correspond to probabilities that the two samples are drawn from the same distribution.

^a Gehan's generalized Wilcoxon test, permutation variance (Feigelson & Nelson 1985; Lavalley et al. 1992).

^b Gehan's generalized Wilcoxon test, hypergeometric variance (Feigelson & Nelson 1985; Lavalley et al. 1992).

^c logrank test (Feigelson & Nelson 1985; Lavalley et al. 1992).

^d Peto & Peto generalized Wilcoxon test (Feigelson & Nelson 1985; Lavalley et al. 1992).

^e Peto & Prentice generalized Wilcoxon test (Feigelson & Nelson 1985; Lavalley et al. 1992).

AGN Luminosity Indicators

TABLE 3
[O III] STATISTICAL TESTS

| Sy1 v. (1) | Sy2 (2) | Sy2, Compton-thin (3) | Sy2, Compton-thick (4) | Sy2, N_H unknown (5) |
|-----------------------|--------------------|--------------------------|---------------------------|---------------------------|
| Gehan, permutation | 0.002 | 0.015 | 0.166 | 3×10^{-4} |
| Gehan, hypergeometric | 2×10^{-4} | 0.015 | 0.164 | 6×10^{-5} |
| logrank | 0.004 | 0.003 | 0.054 | 6×10^{-4} |
| Peto-Peto | 0.002 | 0.003 | 0.054 | 3×10^{-4} |
| Peto-Prentice | 6×10^{-4} | ... | ... | 2×10^{-4} |

NOTE. — Col. (1): Seyfert types 1.0–1.5. 18 objects, 0 upper limits. Col. (2): Seyfert types 1.8–2. 71 objects, 1 upper limit. 1 object with no data (NGC4945). Col. (3): Seyfert types 1.8–2, $N_H < 1 \times 10^{-24} \text{ cm}^{-2}$. 24 objects, 0 upper limits. Col. (4): Seyfert types 1.8–2, $N_H > 1 \times 10^{-24} \text{ cm}^{-2}$. 18 objects, 0 upper limits, 1 object with no data (NGC4945). Col. (5): Seyfert types 1.8–2, N_H unknown. 29 objects, 1 upper limit. The values in Columns 2–5 correspond to probabilities that the two samples are drawn from the same distribution. The Peto & Prentice Wilcoxon test reduces to Gehan's Wilcoxon test when there are no upper limits.

TABLE 4
6 CM STATISTICAL TESTS

| Sy1 v. (1) | Sy2 (2) | Sy2, Compton-thin (3) | Sy2, Compton-thick (4) | Sy2, N_H unknown (5) |
|-----------------------|------------|--------------------------|---------------------------|---------------------------|
| Gehan, permutation | 0.191 | 0.682 | 0.786 | 0.023 |
| Gehan, hypergeometric | 0.172 | 0.682 | 0.787 | 0.017 |
| logrank | 0.078 | 0.517 | 0.677 | 0.006 |
| Peto-Peto | 0.188 | 0.682 | 0.774 | 0.021 |
| Peto-Prentice | 0.197 | 0.685 | 0.775 | 0.021 |

NOTE. — Col. (1): Seyfert types 1.0–1.5. 18 objects, 1 upper limit. (2): Seyfert types 1.8–2. 71 objects, 8 upper limits. Col. (3): Seyfert types 1.8–2, $N_H < 1 \times 10^{-24} \text{ cm}^{-2}$. 24 objects, 1 upper limit. Col. (4): Seyfert types 1.8–2, $N_H > 1 \times 10^{-24} \text{ cm}^{-2}$. 18 objects, 0 upper limits. Col. (5): Seyfert types 1.8–2, N_H unknown. 29 objects, 7 upper limits. The values in Columns 2–5 correspond to probabilities that the two samples are drawn from the same distribution.

TABLE 5
2–10 KEV STATISTICAL TESTS

| Sy1 v. (1) | Sy2 (2) | Sy2, Compton-thin (3) | Sy2, Compton-thick (4) | Sy2, N_H unknown (5) |
|-----------------------|----------------------|--------------------------|---------------------------|---------------------------|
| Gehan, permutation | 1×10^{-5} | 0.057 | 3×10^{-5} | $< 1 \times 10^{-7}$ |
| Gehan, hypergeometric | $< 1 \times 10^{-7}$ | 0.058 | 9×10^{-6} | $< 1 \times 10^{-7}$ |
| logrank | $< 1 \times 10^{-7}$ | 0.015 | 3×10^{-6} | $< 1 \times 10^{-7}$ |
| Peto-Peto | 1×10^{-5} | 0.015 | 3×10^{-5} | $< 1 \times 10^{-7}$ |
| Peto-Prentice | 3×10^{-6} | ... | 1×10^{-5} | $< 1 \times 10^{-7}$ |

NOTE. — Col. (1): Seyfert types 1.0–1.5. 18 objects, 0 upper limits. Col. (2): Seyfert types 1.8–2. 71 objects, 9 upper limits. 8 objects with no data. Col. (3): Seyfert types 1.8–2, $N_H < 1 \times 10^{-24} \text{ cm}^{-2}$. 24 objects, 0 upper limits. Col. (4): Seyfert types 1.8–2, $N_H > 1 \times 10^{-24} \text{ cm}^{-2}$. 18 objects, 1 upper limit. Col. (5): Seyfert types 1.8–2, N_H unknown. 29 objects, 8 upper limits, 8 objects with no data. The values in Columns 2–5 correspond to probabilities that the two samples are drawn from the same distribution. The Peto & Prentice Wilcoxon test reduces to Gehan's Wilcoxon test when there are no upper limits.